

# Carbon Nanotube Template Assisted Synthesis of Zinc Ferrite Nanochains

Li Zhang<sup>a,b</sup>, Yi Wang<sup>a</sup>, Qing-Qing Ni<sup>a,c</sup> \*

<sup>a</sup> Faculty of Textile Science & Technology, Shinshu University, 3-15-1 Tokida, Ueda 386-8567, Japan

<sup>b</sup> Faculty of Engineering, Shinshu University, 4-17-1 Wakasato, Nagano 380-8553, Japan

<sup>c</sup> Institute of Road & Bridge Engineering, Dalian Maritime University, Linghai Road, Dalian 116026, P.R. China

## Abstract

We synthesized zinc ferrite nanochains, assembled from nanoparticles, using a carbon nanotubes (CNTs) template method. The resulting nanochains were systematically characterized with respect to crystal structure, morphology, elemental composition, magnetic properties and specific surface area by X-ray diffraction (XRD), transmission electron microscopy (TEM), field emission scanning electron microscopy (FESEM), X-ray photoelectron spectroscopy (XPS), superconducting quantum interference device (SQUID) magnetometry, and the N<sub>2</sub> adsorption method. The morphology results showed that the zinc ferrite particles with diameters of 10–20 nm were structurally linked to form nanochains. The magnetic property investigation indicated that the zinc ferrite nanochains exhibited ferromagnetic behavior and possessed a saturation magnetization of 45.4 emu/g at 300 K. We addressed the growth mechanism by analyzing the experimental conditions and characterization results. This method may be applicable to synthesizing other metal oxide nanochains as well.

**Keywords:** magnetic materials; nanostructures; energy spectroscopy for chemical analysis (ESCA); crystal structure.

---

\* Corresponding author. Tel.: +81 268 215438; fax: +81 268 215438.  
E-mail address: niqq@shinshu-u.ac.jp (Qing-Qing Ni)

## 1. Introduction

Nanoscale magnetic ferrite materials have attracted much attention over the past few decades due to their physical properties and technological applications [1–8]. Among the ferrite family, zinc ferrite ( $\text{ZnFe}_2\text{O}_4$ ) is of particular interest because it shows many unusual properties very different from the bulk material, especially its magnetic properties [9,10]. Accordingly, researchers have addressed many basic issues of the properties of  $\text{ZnFe}_2\text{O}_4$  nanostructures and have synthesized a series of one-dimensional (1D)  $\text{ZnFe}_2\text{O}_4$  nanostructures [9–19]. Hochepeid et al. [9] first reported the fabrication of nonstoichiometric zinc ferrite nanocrystals and studied their unusual magnetic properties, which differed from other ferrite nanoparticles. Yao et al. [10] developed a thermal decomposition route of metal surfactant complexes to synthesize  $\text{ZnFe}_2\text{O}_4$  nanocrystals with an average particle size of 9.8 nm. Kundu et al. [11] synthesized  $\text{ZnFe}_2\text{O}_4$  nanoparticles by a coprecipitation technique using urea. Recently, Zhang et al. [18] and Liu et al. [19] prepared  $\text{ZnFe}_2\text{O}_4$  nanotubes using an anodic aluminum oxide (AAO) template. These studies have had an enormous impact on nanotechnology and have demonstrated the potential of  $\text{ZnFe}_2\text{O}_4$  nanostructures in a variety of applications.

Despite the above-mentioned efforts, a 1D chainlike  $\text{ZnFe}_2\text{O}_4$  structure has not yet been reported to date. The nanochain, a typical 1D assembly of nanoparticles, is a new member of the nanostructure family [20–22]. Generally, the preparation methods of nanochains can be classified into two main strategies: self-assembly [23–30] and the template-assisted approach [31–34]. Generally, self-assembly requires more rigorous conditions; for the template-assisted approach, it is difficult to completely remove the template (such as an AAO template) and to control the diameter of products smaller than 100 nm. Recently, researchers have considered carbon nanotubes (CNTs) to be an ideal template for the synthesis of 1D nanostructures, hoping that they can overcome the disadvantages of templates [35,36].

In this paper, we report a novel and facile approach to synthesize  $\text{ZnFe}_2\text{O}_4$  nanochains using layer-by-layer (LBL) assembly on a CNT template in combination with subsequent calcination. LBL assembly is based on the electrostatic attraction

between charged species, and it has been widely used to prepare inorganic and hybrid hollow spheres, metal oxide nanotubes, and core-shell nanostructures [37–42]. We now present its use to synthesize zinc ferrite nanochains. Moreover, we also discuss the possible synthesis mechanism. This preparation route should be an effective strategy to prepare other 1D metal oxide nanochains and should pave the way for a wide range of potential applications of zinc ferrite nanochains.

## **2. Experimental**

### **2.1 Synthesis**

We used multi-walled carbon nanotubes with diameters of 20–40 nm (Wako Pure Chemical Industries Ltd., Japan) as received. All other chemical reagents were of analytical grade and were used without further purification. In a typical procedure, 30 mg CNTs were sonicated for 1 h in 50 mL of 1 M NaCl solution, then added 100 mg poly(diallyldimethylammonium chloride) (PDDA), and stirred for 1 h. Subsequently, we substantially removed the excess PDDA by six repeated centrifugation-washing processes. Similarly, the poly(styrenesulfonate) (PSS) layers were then coated on the PDDA-CNTs to obtain PSS/PDDA-CNTs. We dispersed a mixed aqueous solution of 1.6 mmol  $\text{Fe}(\text{NO}_3)_3$  and 0.8 mmol  $\text{Zn}(\text{NO}_3)_2$  in the PSS/PDDA-CNT solution and stirred the mixture for 2 h. The KOH solution was then added dropwise to the solution until the pH reached 8. In this way,  $\text{Fe}^{3+}$  and  $\text{Zn}^{2+}$  precipitated with KOH to attach to the surface of the PSS/PDDA-CNTs. We centrifuged the resulting black products ( $\text{ZnFe}_2(\text{OH})_8/\text{PSS}/\text{PDDA-CNTs}$ ), washed them with distilled water and ethanol, and then dried them at 80°C overnight. The products were heated to 550°C at the rate of 5°C/min and then calcinated at 550°C for 4 h, to remove the polyelectrolyte layers and CNTs as well as the crystallization from metal hydroxides to  $\text{ZnFe}_2\text{O}_4$ .

### **2.2 Characterization**

We imaged the samples with field emission scanning electron microscopy (FESEM, Hitachi S-5000, 20 kV) and transmission electron microscopy (TEM, JEOL JEM-2010, 200 kV). The crystal structures of the samples were characterized by

X-ray powder diffraction (XRD) using a Rigaku Geigerflex 2028 diffractometer with Cu K $\alpha$  radiation ( $\lambda = 1.5418 \text{ \AA}$ ). X-ray photoelectron spectroscopy (XPS) analysis was performed on a Kratos Axis Ultra DLD X-ray photoelectron spectrometer using a standard Mg K $\alpha$  (1256.6 eV) X-ray source (10 mA, 15 kV) and low-energy electron flooding for charge compensation, and all binding energies were referred to C 1s at 285.0 eV. Magnetic measurements were carried out with a commercial superconducting quantum interference device (SQUID) magnetometer (Quantum Design, MPMS). Hysteresis loops were measured at 300 K in a magnetic field in the range of  $\pm 10$  kOe. We measured the specific surface area with the N<sub>2</sub> adsorption method (Micrometrics Gemini, Shimadzu) after degassing the sample at 150°C for 5 h.

### 3. Results and Discussion

We characterized the morphologies of pristine CNTs and the products (ZnFe<sub>2</sub>(OH)<sub>8</sub>/PSS/PDDA/CNTs) by FESEM and TEM as shown in Figure 1. The pristine CNTs (Figure 1a) have diameters of 20–40 nm and have a uniform and flattened interface. From the image (Figure 1b) of the products, we can observe a large quantity of rough CNTs with approximate diameters of 30–50 nm. This phenomenon can also be detected through the TEM image of the products (Figure 1c). Moreover, no obvious flocculent precipitate appears in the image except for on the surface of the CNTs because the metal hydroxides were mainly coated on the PSS/PDDA/CNTs due to the process of electrostatic attraction and coprecipitation. The high resolution TEM image (Figure 1d) of an individual CNT clearly indicates that the coated layers are amorphous with a thickness of about 5–10 nm.

Researchers have reported that CNTs can be oxidized to CO<sub>2</sub> at temperatures above 400°C. Therefore, after calcinating the products at 550°C for 4 h, the polyelectrolyte layers and CNTs were thoroughly removed and the amorphous metal hydroxides were crystallized into ZnFe<sub>2</sub>O<sub>4</sub>. Figure 2 shows the typical XRD patterns of the products before and after calcination. There are no obvious diffraction peaks before calcination because the attached layers were amorphous, which agreed well

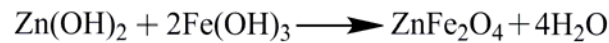
with the TEM analysis. However, after calcination, a set of peaks appear, and all of them matched well with cubic  $\text{ZnFe}_2\text{O}_4$  (JCPDS 22-1012). A relatively broadened diffraction peak indicated that the  $\text{ZnFe}_2\text{O}_4$  nanomaterials had a quite small crystal size. We calculated the particle size using the Scherer formula,  $D = 0.89\lambda/(\beta\cos\theta)$ , where  $\lambda$  is the X-ray wavelength (1.5418 Å),  $\theta$  is the Bragg diffraction angle, and  $\beta$  is the full width at half maximum. The particle diameter was determined as 10.2 nm from the XRD peak of (311).

Figure 3 shows the FESEM image, TEM image, and selected area electron diffraction (SAED) patterns of the  $\text{ZnFe}_2\text{O}_4$  nanomaterials. Figure 3a clearly shows that the products consist of chainlike structures, which was formed from ample spherical nanoparticles. The TEM image (Figure 3b) reveals that the particles were structurally linked to form nanochains. The particles had a uniform size with diameters of 10–20 nm, which was in good agreement with the estimated value by XRD analysis. The corresponding SAED pattern, taken from Figure 3b (see insert), indicates that the nanochains were composed of crystallized  $\text{ZnFe}_2\text{O}_4$  nanoparticles. The diffraction rings could be indexed to cubic  $\text{ZnFe}_2\text{O}_4$ , and the result confirmed the XRD result. A typical high magnification TEM image (Figure 3c) of a  $\text{ZnFe}_2\text{O}_4$  single nanoparticle revealed the crystalline nature of  $\text{ZnFe}_2\text{O}_4$  nanochains. The distances between the two adjacent planes were 0.259 nm and 0.211 nm, corresponding to the (311) planes and (400) planes of cubic  $\text{ZnFe}_2\text{O}_4$  (JCPDS 22-1012), respectively.

To determine the surface compositions and the chemical states of zinc element, we carried out XPS analysis and present the typical XPS spectra in Figure 4. Survey scans (Figure 4a) of the two samples identified the presence of carbon (C 1s), oxygen (O 1s), iron (Fe 2s, 2p, and 3p), and zinc (Zn 2p, 3s, and 3p). The concentration of carbon clearly decreased after calcination because the polyelectrolyte layers and CNTs were oxidized to  $\text{CO}_2$  during the calcination process. Figure 4b shows the high resolution spectra of Zn 2p. For the sample before calcination, double peaks with binding energies of 1022.8 and 1045.9 eV correspond to Zn 2p<sub>3/2</sub> and Zn 2p<sub>1/2</sub> of the zinc hydroxide, respectively [43]. However, the binding energies of Zn 2p shifted toward the low energy side after calcination; the values were 1021.4 eV for Zn 2p<sub>3/2</sub>

and 1044.4 eV for Zn 2p<sub>1/2</sub>. The shift could be attributed to the crystallization of Zn/Fe hydroxides into ZnFe<sub>2</sub>O<sub>4</sub>. The Zn 2p<sub>3/2</sub> peak at 1021.4 eV was ascribed to the formation of ZnFe<sub>2</sub>O<sub>4</sub> with a zinc atom occupying the tetrahedral site [43]. On the other hand, Bera et al. [44] have reported that the Zn 2p<sub>3/2</sub> peak shifted to about 1023.2 eV when zinc atoms occupy the octahedral site in ZnFe<sub>2</sub>O<sub>4</sub>. Thus, we assumed that the small peak with a binding energy of 1022.9 eV, separated from Zn 2p<sub>3/2</sub> of ZnFe<sub>2</sub>O<sub>4</sub>, was due to the incorporation of Zn<sup>2+</sup> ions at the octahedral site.

Based on the experimental conditions and the above-mentioned analysis, we propose a formation mechanism for our ZnFe<sub>2</sub>O<sub>4</sub> nanochains (Figure 5). During the first stage, the LBL assembly of PDDA and PSS on the CNT surface prepared PSS/PDDA-CNTs. Then, Fe<sup>3+</sup> and Zn<sup>2+</sup> ions were absorbed onto the surface of PSS/PDDA-CNTs to form ZnFe<sub>2</sub>(OH)<sub>8</sub>/PSS/PDDA-CNTs complex due to the process of electrostatic adsorption and coprecipitation. In the calcination stage, the increased temperature led to many splits within the cylindrical combined layers (polyelectrolyte and Zn/Fe hydroxides) and divided them into many separated segments. Moreover, the edges of the separated segments could be bent against the CNT surface due to the improved temperature. Meanwhile, because of the thermal instability of the Zn/Fe hydroxides, the first batch of ZnFe<sub>2</sub>O<sub>4</sub> nanocrystals formed when a suitable temperature was reached. The formation of ZnFe<sub>2</sub>O<sub>4</sub> nanoparticles may be ascribed to the dehydration of Fe(OH)<sub>3</sub> and Zn(OH)<sub>2</sub>, and the reaction can be described as follows:



Once the ZnFe<sub>2</sub>O<sub>4</sub> nanocrystals formed, their morphology was relatively unchanged and the ZnFe<sub>2</sub>O<sub>4</sub> beads experienced continuous growth afterward. Because the splits avoided the agglomeration of nanoparticles located on different segments, the nanoparticles on the same segment could only connect one another to form linear chains. Finally, ZnFe<sub>2</sub>O<sub>4</sub> nanochains were obtained by the calcination.

Generally, the competing weak forces (such as steric, van der Waals, entropy, and magnetostatic) that determine self-assembly and the resulting organization of nanoparticle, greatly depends on the particle properties [45,46]. In our case, the

nanoparticles were ferromagnetic, indicating that the magnetostatic interaction was much more significant than other forces.

Among all the properties of  $\text{ZnFe}_2\text{O}_4$  nanochains, the magnetic properties and high surface area are necessary from the point of view of practical applications. Figure 6 indicates the magnetic properties of the synthesized nanochains at room temperature. The value of saturation magnetization was about 45.4 emu/g at 300 K. Bulk zinc ferrite has a completely normal spinel structure with  $\text{Zn}^{2+}$  in the tetrahedral sites (A sites) and  $\text{Fe}^{3+}$  in the octahedral sites (B sites). Thus, there is no superexchange interaction between A-B sites leading to strong paramagnetism and a very low ordering temperature. When the size of zinc ferrite decreases to the nanoscale, certain degrees of inversion (a fraction of  $\text{Zn}^{2+}$  in the B sites and  $\text{Fe}^{3+}$  in the A sites) can be achieved by many different synthetic methods [10–17], leading to ferrimagnetic coupling between the octahedral and tetrahedral sublattices and resulting in unusual magnetic properties as compared to the bulk material. In Table 1, we list reported values of saturation magnetization ( $M_s$ ) for zinc ferrite nanostructures prepared by various methods. The broad range of values of  $M_s$  in Table 1 confirmed the fact that the magnetic property strongly depends on the synthetic method used. Our value of  $M_s$  indicated that the rearrangement of  $\text{Fe}^{3+}$  and  $\text{Zn}^{2+}$  between A and B sites occurred during synthesis, and the result agreed well with the XPS result. Moreover, we measured the specific surface area with the  $\text{N}_2$  adsorption method. The  $\text{N}_2$  adsorption-desorption curve in Figure 6b shows a hysteresis loop with a Brunauer-Emmett-Teller (BET) surface area of 78.7  $\text{m}^2/\text{g}$ . The high surface area of the nanochains should be a crucial parameter for their future application.

#### **4. Conclusion**

In summary, we have developed a novel approach to synthesize zinc ferrite nanochains using layer-by-layer assembly on CNT templates in combination with subsequent calcination. The morphological analysis indicated that the resultant chainlike nanostructures were composed of uniform nanoparticles with approximate diameters of 10 nm. On the basis of the experimental results, we proposed a possible

explanation of the growth mechanism. From our magnetization data, we inferred a ferromagnetic structure of the nanochains with a saturation magnetization of 45.4 emu/g at 300 K.

### **Acknowledgements**

This work was partly supported by Grant-in-Aid for Global COE Program and CLUSTER (the second stage) by the Ministry of Education, Culture, Sports, Science, and Technology, Japan.

## References

- [1] V.S. Coker, N.D. Telling, G. van der Laan, R.A.D. Patrick, C.I. Pearce, E. Arenholz, F. Tuna, R.E.P. Winpenny, J.R. Lloyd, ACS Nano 3 (2009) 1922.
- [2] L. Chen, C. Zhao, J. Bai, Chem. Lett. 38 (2009) 276.
- [3] S. Yu, M. Yoshimura, Chem. Mater. 12 (2009) 3805.
- [4] T.O. Richard, S.A. German, S.H. Mikael, U.W. Gedde, F. Lindberg, S.J. Savage, Chem. Mater. 17 (2005) 5109.
- [5] C. Barcena, A.K. Sra, G.S. Chaubey, C. Khemtong, J.P. Liu, J. Gao, Chem. Commun. 19 (2008) 2224.
- [6] S. Bhattacharyya, J.P. Salvetat, R. Fleurier, A. Husmann, T. Cacciaguerra, M.L. Saboungi, Chem. Commun. 38 (2005) 4818.
- [7] D.R. Patil, B.K. Chougule, Mater. Chem. Phys. 117 (2009) 35.
- [8] S.E. Shirsath, B.G. Toksha, K.M. Jadhav, Mater. Chem. Phys. 117 (2009) 163.
- [9] J.F. Hochepped, P. Bonville, M.P. Pileni, J. Phys. Chem. B 104 (2000) 905.
- [10] C. Yao, Q. Zeng, G.F. Goya, T. Torres, J. Liu, H. Wu, M. Ge, Y. Zeng, Y. Wang, J.Z. Jiang, J. Phys. Chem. C 111 (2007) 12274.
- [11] A. Kundu, C. Upadhyay, H.C. Verma, Phys. Lett. A 311 (2003) 410.
- [12] R.D.K. Misra, S. Gubbala, A. Kale, W.F. Egelhoff Jr, Mater. Sci. Eng. B 111 (2004) 164.
- [13] N. Wakiya, K. Muraoka, T. Kadowaki, T. Kiguchi, N. Mizutani, H. Suzuki, K. Shinozaki, J. Magn. Magn. Mater. 310 (2007) 2546.
- [14] M. Sivakumar, T. Takami, H. Ikuta, A. Towata, K. Yasui, T. Tuziuti, T. Kozuka, D. Bhattacharya, Y. Iida, J. Phys. Chem. B 110 (2006) 15234.
- [15] S.D. Shenoy, P.A. Joy, M.R. Anantharaman, J. Magn. Magn. Mater. 269 (2004) 217.
- [16] H. Xue, Z. Li, X. Wang, X. Fu, Mater. Lett. 61 (2007) 347.
- [17] H.S. Ammar, N. Jouini, F. Fievet, Z. Beji, L. Smiri, P. Moline, M. Danot, J.M. Greneche, J. Phys.: Condens. Matter 18 (2006) 9055.
- [18] G. Zhang, C. Li, F. Cheng, J. Chen, Sensor Actual B Chem. 120 (2007) 403.

- [19] F. Liu, X. Li, Q. Zhao, Y. Hou, X. Quan, G. Chen, *Acta. Mater.* 57 (2009) 2684.
- [20] M.A. Rafiq, Z.A.K Durrani, H. Mizuta, A. Colli, P. Servati, A.C. Ferrari, W.I. Milne, S.J. Oda, *Appl. Phys.* 103 (2008) 053705.
- [21] H. Kohno, S. Takeda, *Appl. Phys. Lett.* 73 (1998) 3144.
- [22] H. Kohno, I. Kikuo, K. Oto, *J. Electron Microsc.* 54 (2005) I15.
- [23] T. Nishinaka, A. Takano, Y. Doi, M. Hashimoto, A. Nakamura, Y. Matsushita, J. Kumaki, E. Yashima, *J. Am. Chem. Soc.* 127 (2005) 8120.
- [24] A. Tang, N.A. Kotov, M. Gierisig, *Science* 297 (2002) 237.
- [25] Z. Tang, B. Ozturk, Y. Wang, N.A. Kotov, *J. Phys. Chem. B* 108 (2004) 6927.
- [26] X.G. Peng, L. Manna, W. Yang, J. Wickham, E. Scher, A. Kadavanich, A.P. Alivisatos, *Nature* 404 (2000) 59.
- [27] X.L. Shi, M.S. Gao, J. Yuan, X.Y. Fang, *Appl. Phys. Lett.* 95 (2009) 163108.
- [28] L. Gao, F. Liang, X. Wen, S. Yang, L. He, W. Zheng, C. Chen, Q. Zhong, *Adv. Funct. Mater.* 17 (2007) 425.
- [29] M. Cao, H. Liu, Y. Chen, B. Wang, J. Zhu, *Sci. China Ser. E* 46 (2003) 104.
- [30] M. Gao, R. Wang, X. Fang, Z. Cui, T. Chang, *Powder Technol.* 115 (2001) 96.
- [31] Y. Li, Z. Wang, X.D. Ma, X.F. Qian, J. Yin, Z.K. Zhu, *J. Solid State Chem.* 177 (2004) 4386.
- [32] X. Wang, P. Gao, J. Li, C.J. Summers, Z.L. Wang, *Adv. Mater.* 14 (2002) 1732.
- [33] G. Malandrino, S.T. Finocchiaro, I.L. Fragala, *J. Mater. Chem.* 14 (2004) 2726.
- [34] M. Chen, L. Gao, *J. Cryst. Growth* 286 (2006) 228.
- [35] B.C. Satishkumar, A. Govindaraj, E.M. Vogel, L. Basumalick, C.N.R. Rao, *J. Mater. Res.* 12 (1997) 604.
- [36] Z. Sun, H. Yuan, Z. Liu, B. Han, X. Zhang, *Adv. Mater.* 17 (2005) 2993.
- [37] N. Du, H. Zhang, B. Chen, X. Ma, Z. Liu, J. Wu, D. Yang, *Adv. Mater.* 19 (2007) 1641.
- [38] G. Decher, *Science* 277 (1997) 1232.
- [39] F. Caruso, R.A. Caruso, H. Möhwald, *Science* 282 (1998) 1111.
- [40] F. Caruso, *Adv. Mater.* 13 (2001) 11.
- [41] S.F. Ai, Q. He, C. Tao, S.P. Zheng, J.B. Li, *Macromol. Rapid Commun.* 26 (2005)

1965.

[42] S.F. Ai, G. Lu, Q. He, J.B. Li, *J. Am. Chem. Soc.* 125 (2003) 11140.

[43] L.S. Dake, D.R. Baer, J.M. Zachara, *Surf. Interface Anal.* 14 (1989) 71.

[44] S. Bera, A.A.M. Prince, S. Velmurugan, P.S. Raghavan, R. Gopalan, G. Panneerselvam, S.V. Narasimhan, *J. Mater. Sci.* 36 (2001) 5379.

[45] B.Y. Geng, J.Z. Ma, X.W. Liu, Q.B. Du, M.G. Kong, L.D. Zhang, *Appl. Phys. Lett.* 90 (2007) 043120.

[46] K.M. Krishnan, A.B. Pakhomov, Y. Bao, P. Blomqvist, Y. Chun, M. Gonzales, K. Griffin, X. Ji, B.K. Roberts, *J. Mater. Sci.* 41 (2006) 793.

## Figure Captions

Figure 1. (a) FESEM image of pristine CNTs and (b-d) morphological, structural characterization of the  $\text{ZnFe}_2(\text{OH})_8/\text{PSS}/\text{PDDA}/\text{CNTs}$  prepared by layer-by-layer assembly and chemical coprecipitation: (b) FESEM image, (c) TEM image, and (d) HRTEM image of an individual CNT.

Figure 2. X-ray diffraction patterns: (a)  $\text{ZnFe}_2(\text{OH})_8/\text{PSS}/\text{PDDA}/\text{CNTs}$  and (b)  $\text{ZnFe}_2\text{O}_4$  nanochain.

Figure 3. Morphological and structure characterizations of the  $\text{ZnFe}_2\text{O}_4$  nanochains: (a) FESEM image, (b) TEM image with the SEAD shown in the inset, and (c) HRTEM image of an individual nanochain.

Figure 4. XPS spectra of  $\text{ZnFe}_2(\text{OH})_8/\text{PSS}/\text{PDDA}/\text{CNTs}$  and  $\text{ZnFe}_2\text{O}_4$  nanochain: (a) survey scan and (b) Zn 2p narrow scan.

Figure 5. Schematic illustration of the synthesis process of  $\text{ZnFe}_2\text{O}_4$  nanochains.

Figure 6. (a) Hysteresis curve of the  $\text{ZnFe}_2\text{O}_4$  nanochain at 300 K and (b)  $\text{N}_2$  adsorption and desorption curves of  $\text{ZnFe}_2\text{O}_4$  nanochains.

Table 1: Reported values of saturation magnetization for zinc ferrite nanostructure synthesized by various methods.

Ms (emug/g)	Temp. (K)	Particle size (nm)	Synthetic method	Ref. no
45.4	300	10	Template Assisted coprecipitation followed by calcination	this work
44.9	300	9.8	thermal decomposition	10
53	10	13	Coprecipitation technique using area	11
8	300	3.1	Reverse micelle technique	12
56.6	300	Thin film	Pulse laser deposition (with magnetic field)	13
25	5	12	Sonochemical emulsification and evaporation	14
20	83	10	Ball milling	15
~10	300	30	self-propagating combustion method	16
78	5	6.6	hydrolysis in a polyol medium	17

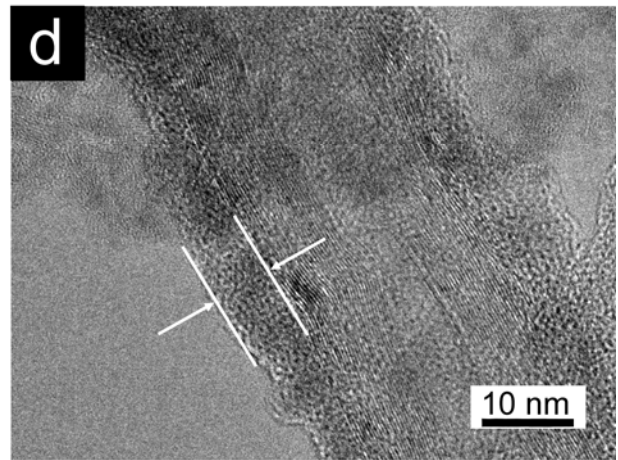
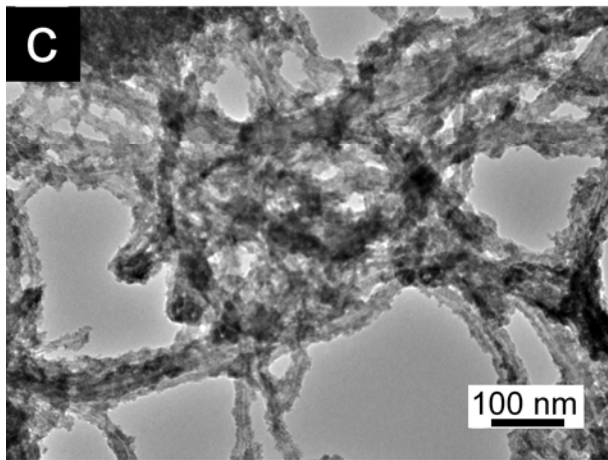
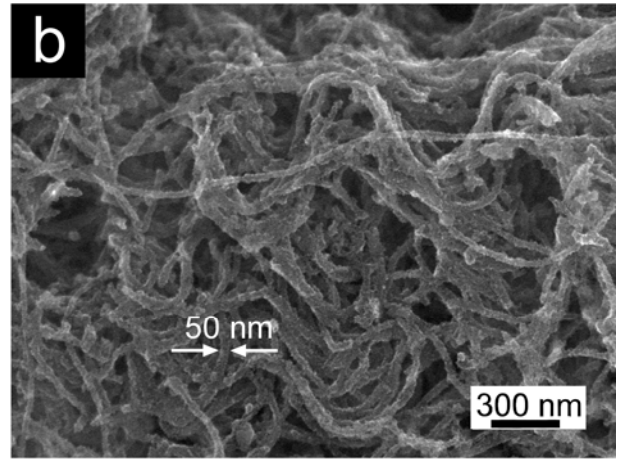
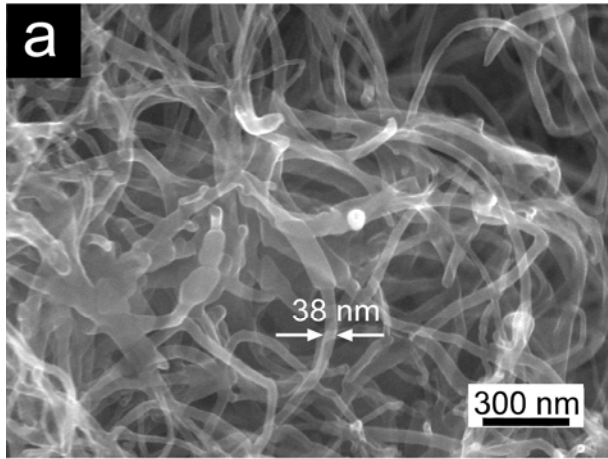


Figure 1.

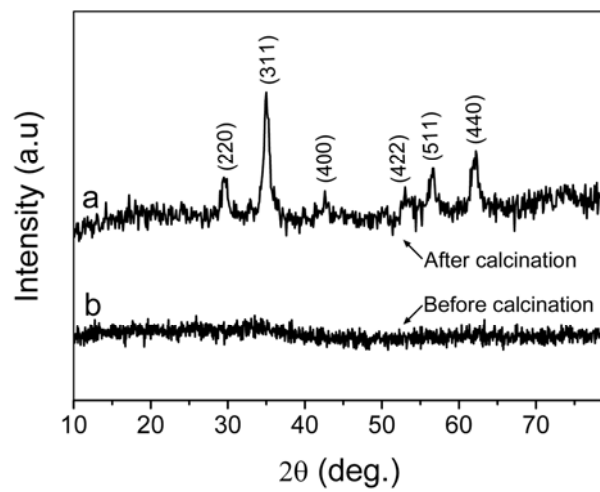


Figure 2.

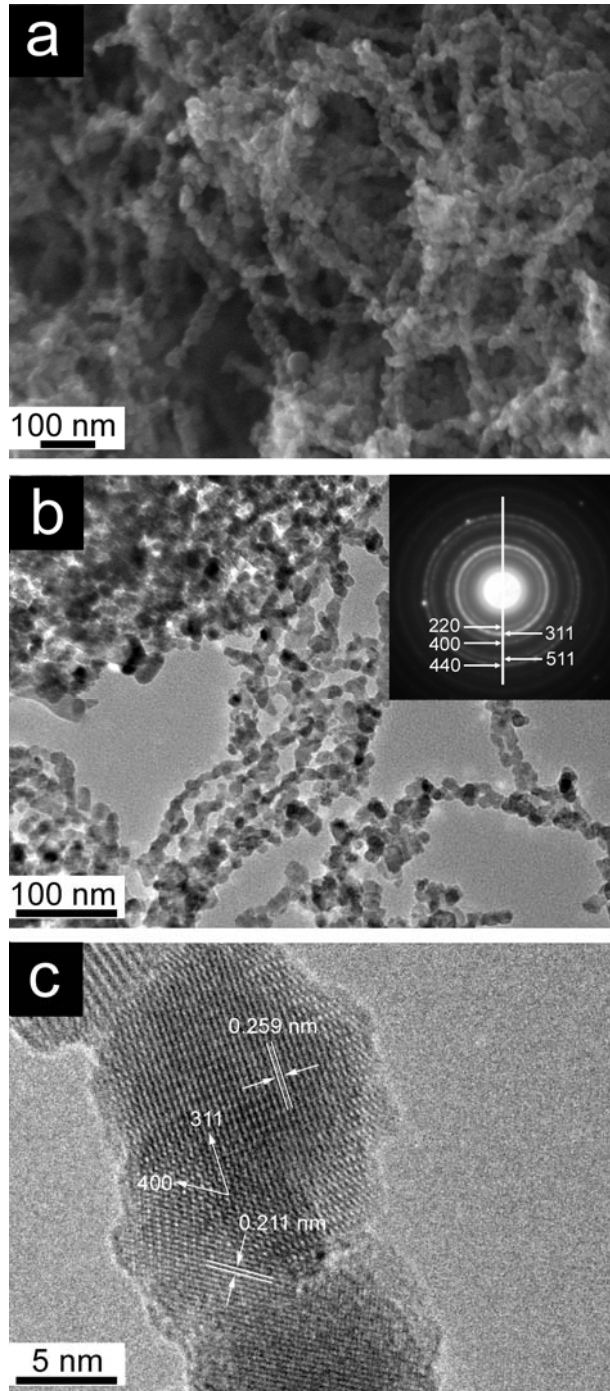


Figure 3.

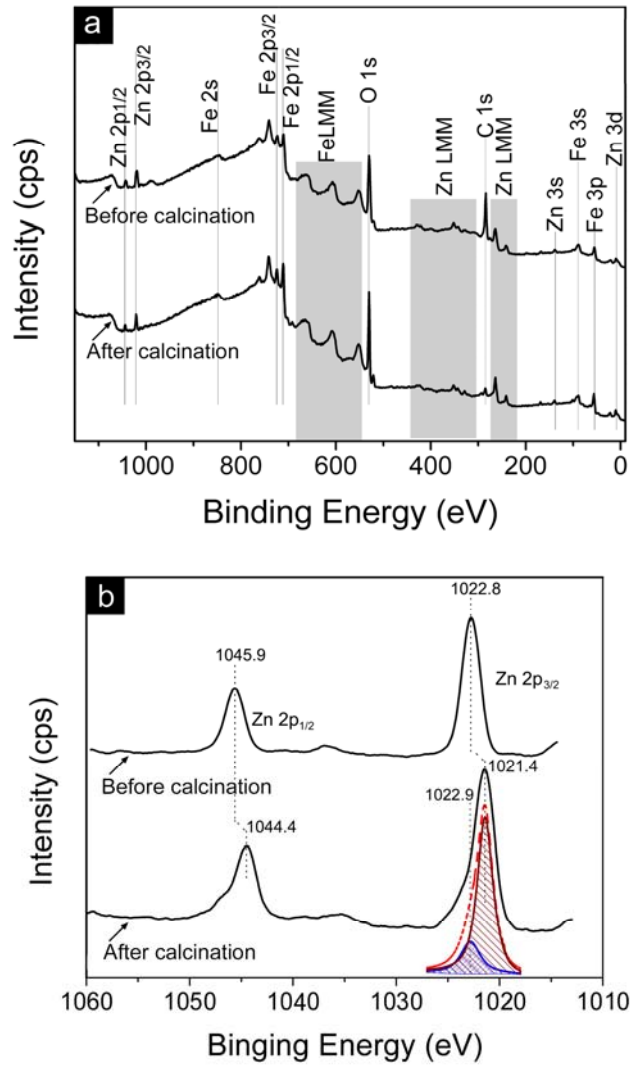


Figure 4.

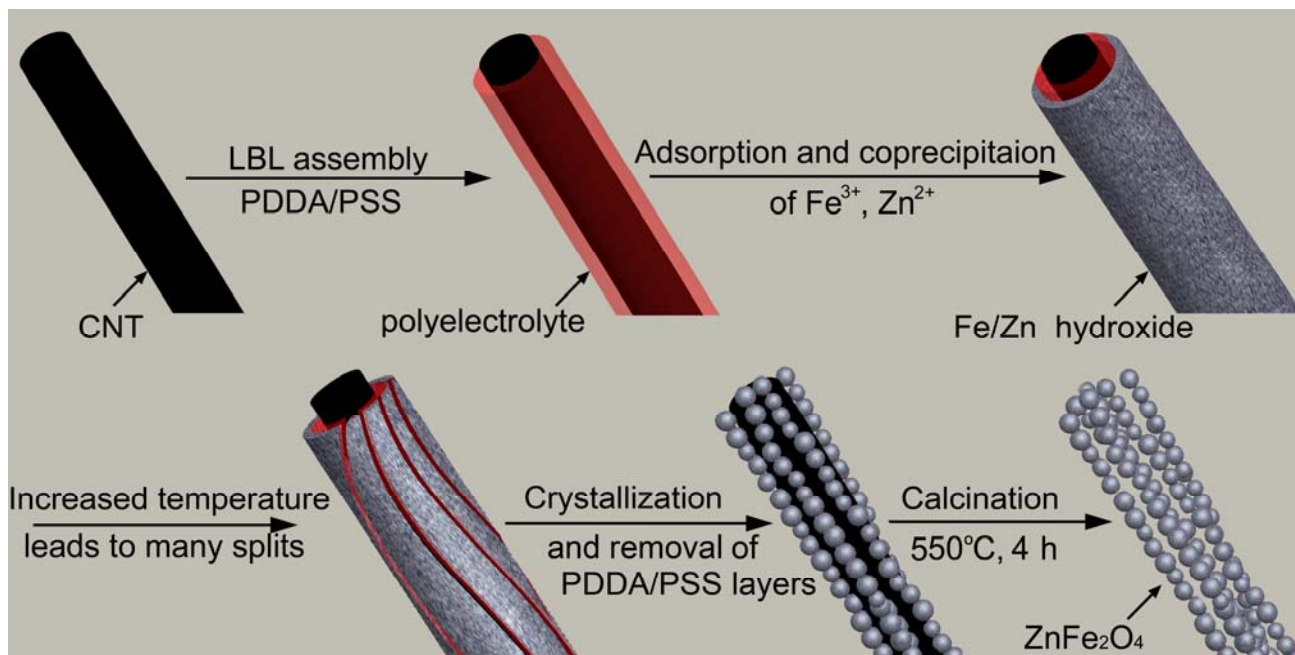


Figure 5.

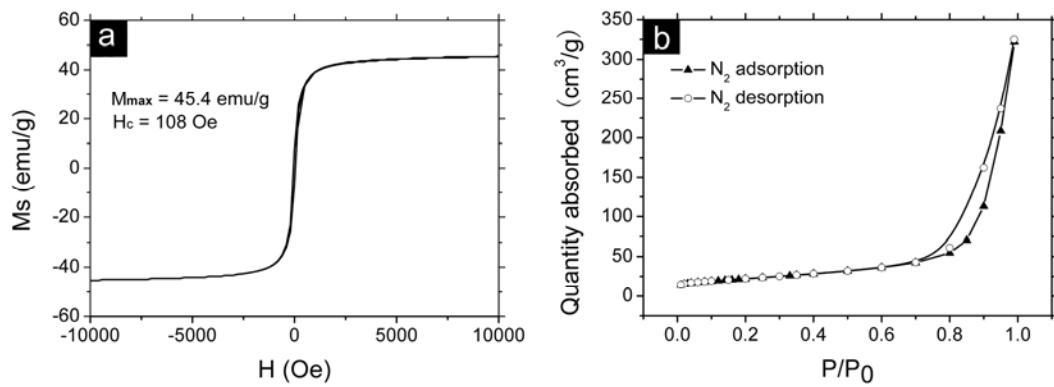


Figure 6.